Research Article | Vol. 28, No. 18 / 31 August 2020 / Optics Express 26041
Optics EXPRESS

Dual-layer achromatic metalens design with an effective Abbe number

MENGMENG LI,[1] SHUAISHUAI LI,[1] LIP KET CHIN,[2,3] YEFENG YU,[1,5] DIN PING TSAI,[4] AND RUSHAN CHEN[1,6]

[1]School of Electronic and Optical Engineering, Nanjing University of Science and Technology, Nanjing 210094, China
[2]School of Electrical and Electronic Engineering, Nanyang Technological University, 639798, Singapore
[3]Center for Systems Biology, Massachusetts General Hospital, Massachusetts 02114, USA
[4]Department of Electronic and Information Engineering, The Hong Kong Polytechnic University, Hung Hom, Hong Kong
[5]yf_yu@njust.edu.cn
[6]eerschen@njust.edu.cn

Abstract: Planar achromatic metalenses with a thickness of the order of wavelength have attracted much attention for their potential applications in ultra-compact optical devices. However, realizing single-layer achromatic metalenses across a wide bandwidth requires that the corresponding meta-atoms have complex cross-sections for correct phase profile and dispersion compensation. Herein, we introduce an effective Abbe number and use lens maker equations to design a dual-layer achromatic metalens in which we compensate the dispersion by using a plano-convex liked metalens combined with a plano-concave liked metalens. The stacked metalens are designed based on simple high refractive index dielectric cylindrical meta-atoms with different radii, which simplify the design and fabrication processes. We demonstrate that a dual-layer achromatic metalens has a small focal length difference across the visible wavelength range and an average focusing efficiency above 50%, which proves that the design method is promising for many potential applications in multi-functional flat optical devices.

1. Introduction

Metasurfaces are widely used for wavefront manipulation in designing planar metalens with high efficiency [1–7]. A planar metalens working in a wide wavelength range is very important for multi-functional integrated optical devices [8,9]. However, metalens is usually suffered from optical dispersion, regardless of whether the corresponding phase delay of meta-atoms is induced by resonance [10–13], geometry-polarization interaction (Pancharatnam-Berry phase) [14–16], propagation mode [9–17], or effective refractive index [18–20]. To mitigate such optical dispersion, metalenses that composed of meta-atoms with several dielectric resonators are designed to compensate for the group delay at corresponding wavelengths [21–24]. For instance, chromatically corrected three-layer metalens are demonstrated [23], in which each layer composes one type of resonator and supports one specific wavelength focusing at the same location. Spatial multiplexing functional metalens is also presented, consisting of a single aperture with different types of meta-atoms for specific wavelength focusing [24,25]. It is achieved by locating the same type of meta-atoms in macroscopic areas of aperture or interleaving different types of meta-atoms in the aperture. However, it remains challenging to design such meta-atoms in a wide continuous wavelength range since the resonance peaks only appear at discretized wavelengths.

Alternatively, single-layer achromatic metalenses that work in a wide bandwidth are designed to compensate optical dispersion by minimizing the phase difference of meta-atoms at selected wavelengths [26–30]. However, the working bandwidth is relatively narrow (60 nm in visible and 140 nm in near-infrared). The phase profile of metalens is decomposed into two parts:

#402478 https://doi.org/10.1364/OE.402478
Journal © 2020 Received 10 Jul 2020; revised 12 Aug 2020; accepted 13 Aug 2020; published 19 Aug 2020

Optics EXPRESS

typical phase profile at reference wavelength and dispersions at the designed wavelengths. To extend the working bandwidth, elaborately designed meta-atoms with complex cross-sections are proposed to satisfy the typical phase profile and compensate the dispersions simultaneously [31–36]. For instance, the Pancharatnam-Berry phase with circularly polarized incident light is usually used to match the typical phase profile, and two [33] or five [35] different meta-atoms are selected to compensate the dispersions at different locations on the metalenses. More polarization-independent meta-atoms are designed to satisfy the two parts [36] to achieve achromatic metalenses.

On the other hand, multi-layer metalenses are proposed for monochromatic aberration correction [37,38]. Compared to single-layer metalenses, multi-layer metalenses have more design freedom, which enables more possible functionalities on the same device. There are several multi-layer achromatic metalens design methods have been reported. A single-layer metalens coupled with a traditional refractive lens is proposed for chromatic aberration correction through artificial meta-atoms [39], an achromatic doublet metalens is designed based on the combination of propagation phase and geometric phase [40], and the cascaded metasurfaces with arbitrary chromatic dispersion is achieved through light trajectories manipulation [41]. In this paper, we introduce an effective Abbe number into the design of dual-layer achromatic metalens (DAML) that consists of a dielectric plano-convex liked metalens (PVML) and a plano-concave liked metalens (PCML). Like the traditional doublet, the optical dispersion is compensated in broadband due to the reverse dispersion properties of PVML and PCML rather than the meta-atoms themselves. Therefore, theoretically, we can use arbitrary meta-atoms for metalens design without considering their phase dispersion.

2. Design theory

The proposed DAML is designed with a PVML and PCML to focus and defocus light beam, respectively, as shown in Figs. 1(a) and (b). The simulation results show that for normal dispersion, the focal length of PVML increases with operating wavelength. Conversely, the negative focal length of PCML decreases with wavelength. Therefore, the PVML and PCML show reverse dispersion and the phase dispersion in the broadband range can be properly compensated by stacking them together, as shown in Figs. 1(c) and (d). Here, D is the diameter of metalens, r is the distance from an arbitrary meta-atom to the center point of metalens, f_1 and f_2 are the focal lengths of the PVML and PCML, d is the distance between PVML and PCML, n_1 and n_2 are the effective indices of cylinders in the surrounding medium, n_3, n_4, and n_5 are the refractive indices of substrates. We introduce an effective Abbe number to describe the dispersion of PVML and PCML and to derive the design procedure of DAML.

When a collimated light beam passes through a metalens, the additional phase delay is introduced in light propagation and the beam is focused on a focal point, as shown in Fig. 1(a). For a metalens with focal length f_1, the required phase profile is described as

$$\varphi(r) = \frac{2\pi}{\lambda}\left(\sqrt{f_1^2 + r^2} - f_1\right) + \Delta\varphi, \tag{1}$$

where r is the distance between an arbitrary point in the lens plane and the center point of the lens, λ is the light wavelength, and $\Delta\varphi$ is the reference phase, which is equal to the phase at the center point ($\Delta\varphi = \varphi(r)|r = 0$).

For a traditional refractive lens in the air with spherical surfaces on both sides, the focal length can be calculated from the lens maker's equation

$$\frac{1}{f} = (n-1)\left[\frac{1}{r_1} - \frac{1}{r_2} + \frac{(n-1)h}{nr_1r_2}\right], \tag{2}$$

where f is the focal length of the lens, n is the refractive index of the lens material, r_1 and r_2 are the radius of curvature of the lens surface closer and farther from the light source, respectively,

Optics EXPRESS

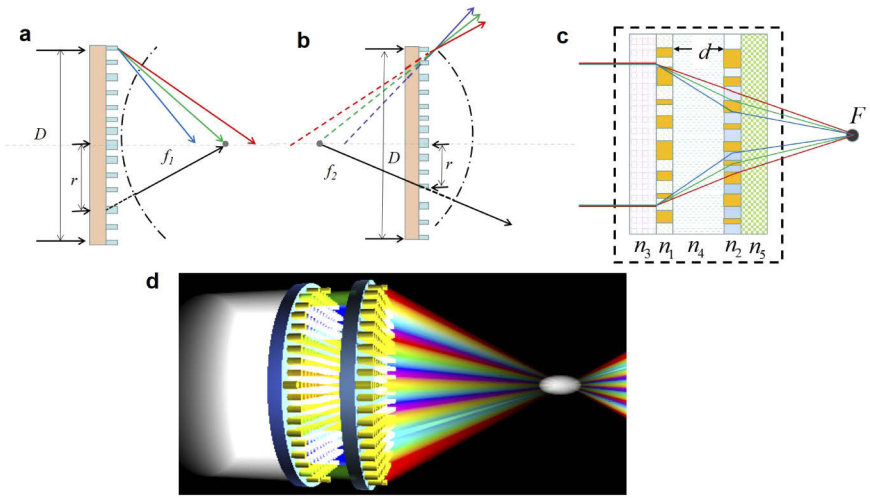

Fig. 1. Schematics illustration of the dual-layer achromatic metalens (DAML). Schematic of (a) a plano-convex liked metalens (PVML) and (b) a plano-concave liked metalens (PCML). (c) The cross-sectional view of the DAML, which includes a pair of PVML and PCML with reverse dispersion properties. (d) The three-dimensional view of the DAML, which focuses a parallel white light beam into a spot when the dispersion is compensated properly.

and h is the thickness of the lens, i.e., the distance along the lens axis between the two surface vertices.

If h is much smaller with respect to r_1 and r_2, the thin lens approximation can be employed. The focal length f of the lens is simplified as

$$\frac{1}{f} = (n_1 - 1)(\frac{1}{r_1} - \frac{1}{r_2}). \tag{3}$$

For our design of PVML or PCML, r_2 is infinite and Eq. (3) can be approximated as

$$\frac{1}{f_i} = (n_i - 1)\frac{1}{r_i} = (n_i - 1)\rho_i, \tag{4}$$

where f_i is the focal length, ρ_i is the equivalent curvature of PVML ($i = 1$) or PCML ($i = 2$).

In traditional achromatic lens design (e.g., doublet), the material dispersion is usually described by using the Abbe number

$$V = \frac{n_D - 1}{n_F - n_C}, \tag{5}$$

where n is the refractive index, and the subscripts D, F, and C represent three pre-determined wavelengths. For the visible wavelength range, they are 589.3 nm, 486.1 nm, and 656.3 nm.

The effective refractive index of the PVML is derived from Eq. (4) as

$$n_1 = 1 + \frac{1}{f_1\rho_1}. \tag{6}$$

When we obtain the effective refractive index from Eq. (6) at three pre-determined wavelengths, the effective Abbe number of the PVML can be expressed as

$$V_1 = \frac{n_{1D} - 1}{n_{1F} - n_{1C}} = \frac{1/f_{1D}\rho_{1D}}{1/f_{1F}\rho_{1F} - 1/f_{1C}\rho_{1C}}. \tag{7}$$

Similar to the refractive lens, we assume that the dispersion of PVML is only determined by the effective refractive index and the equivalent curvature ρ_1 is independent of the wavelength.

Optics EXPRESS

As a result, the effective Abbe number of PVML is written as

$$V_1 = \frac{f_{1F} f_{1C}}{f_{1D}(f_{1C} - f_{1F})}. \tag{8}$$

For the PCML with the focal length of f_2 as shown in Fig. 1(b), the required phase profile is defined as

$$\varphi(r) = \frac{2\pi}{\lambda}\left(f_2 - \sqrt{f_2^2 + r^2 - \left(\frac{D}{2}\right)^2}\right) + \Delta\varphi, \tag{9}$$

where r is the distance between an arbitrary point in the lens plane and the center point of the lens, D is the diameter of PCML, λ is the wavelength, and $\Delta\varphi$ is a reference phase at the edge ($\Delta\varphi = \varphi(r)|r = D/2$). Similar to the derivation of Eq. (8), the effective Abbe number V_2 of PCML is

$$V_2 = \frac{f_{2F} f_{2C}}{f_{2D}(f_{2C} - f_{2F})}. \tag{10}$$

The focal length of DAML, f_t, is determined by f_1,f_2, and d in the equation of two combined thin lens as

$$\frac{1}{f_t} - \left(\frac{1}{f_1} + \frac{1}{f_2} - \frac{d}{f_1 f_2}\right) = 0. \tag{11}$$

In contrast to PVML, the focal length of PCML cannot be obtained from numerical computation directly, since PCML does not have a real focal spot. Two methods can be employed to calculate the focal length. The first one is to fit the focal length with Eq. (9). In this method, the input parameters are the phase profile $\varphi(r)$ after the PCML with a plane wave incidence, the diameter D, and the wavelength λ. The focal length f_2 can be fitted out automatically with a nonlinear least square method. The second method is to calculate the focal length with adjoint electromagnetic simulations [42,43], as shown in Fig. 1(b). There would be a real focal point at the left side of PCML and f_2 obtained directly.

We substitute Eq. (4) into Eq. (11), and rewrite it as

$$\frac{1}{f_t} = (n_1 - 1)\rho_1 - (n_2 - 1)\rho_2 + (n_1 - 1)\rho_1(n_2 - 1)\rho_2 d. \tag{12}$$

Achromatic metalens means that f_t is independent of the wavelength in a wide range. Therefore, for ideal conditions, the differentiation of the left side of Eq. (12) (defined as the dispersion of DAMLΔ) is equal to zero

$$\Delta = \frac{\partial}{\partial\lambda}\left(\frac{1}{f_t}\right) = 0. \tag{13}$$

By substituting Eq. (12) into Eq. (13) and considering the previous assumption that dispersion only comes from the effective refractive index, Δ in Eq. (13) can be written as

$$\Delta = \rho_1 \left.\frac{\partial n_1}{\partial\lambda}\right|_{\lambda=\lambda_D} - \rho_2 \left.\frac{\partial n_2}{\partial\lambda}\right|_{\lambda=\lambda_D} + \rho_1\rho_2 d\left[(n_2 - 1)\left.\frac{\partial n_1}{\partial\lambda}\right|_{\lambda=\lambda_D} + (n_1 - 1)\left.\frac{\partial n_2}{\partial\lambda}\right|_{\lambda=\lambda_D}\right], \tag{14a}$$

where

$$\left.\frac{\partial n_1}{\partial\lambda}\right|_{\lambda=\lambda_D} \approx \frac{n_{1F} - n_{1C}}{\lambda_F - \lambda_C}, \tag{14b}$$

$$\left.\frac{\partial n_2}{\partial\lambda}\right|_{\lambda=\lambda_D} \approx \frac{n_{2F} - n_{2C}}{\lambda_F - \lambda_C}. \tag{14c}$$

Optics EXPRESS

As noted in Eqs. (14b) and (14c), we assume that the refractive index has a linear relationship with respect to the wavelength. Therefore, we can rewrite Eq. (14a) as

$$\Delta = \rho_1 \frac{n_{1F} - n_{1C}}{\lambda_F - \lambda_C} - \rho_2 \frac{n_{2F} - n_{2C}}{\lambda_F - \lambda_C} + \rho_1 \rho_2 d \left[(\mathrm{n}_2 - 1) \frac{\mathrm{n}_{1F} - n_{1C}}{\lambda_F - \lambda_C} + (n_1 - 1) \frac{n_{2F} - n_{2C}}{\lambda_F - \lambda_C} \right]. \quad (15)$$

By considering Eqs. (4) and (5), for achromatic metalens, it can be simplified as

$$\Delta' = \Delta(\lambda_F - \lambda_C) = \frac{1}{V_1} \frac{1}{f_1} + \frac{1}{V_2} \frac{1}{f_2} - d \left(\frac{1}{V_1} \frac{1}{f_1} \frac{1}{f_2} + \frac{1}{V_2} \frac{1}{f_1} \frac{1}{f_2} \right) = 0. \quad (16)$$

Obviously, for Eq. (16), when we have a pre-designed PVML with a fixed effective Abbe number V_1 and a focal length f_1, the PCML with desired effective Abbe number V_2 and desired focal length f_2 can be directly solved from Eqs. (11) and (16) if d is fixed as a constant. However, in most cases, the solution of V_2 and f_2 cannot match with each other for a real designed PCML (we will discuss this in more detail in the results section). Thus, the design procedure is transformed into an optimization problem, which means that, to design a DAML with a focal length of f_t, we have to find a pair of metalenses with V_1, f_1, V_2, f_2 from all possible cases of PCML and PVML to satisfy Eq. (11) and to minimize the dispersion $|\Delta'|$.

All full-wave simulations in this work are implemented by using the finite-difference time-domain (FDTD) method. Without losing generality, all our designs without specific explanations are limited to cylindrical metalens, which focuses the incident light on a line [44].

3. Results and discussions

3.1. Meta-atoms

Meta-atom is the foundation of metalens design. As mentioned in the introduction, there are four types of meta-atoms [10–20] based on different mechanisms of phase delay generation. We use a high refractive index cylinder as the meta-atom for metalens design, which introduces phase delay through waveguide mode. It has a simple design, a relatively broader phase response, and is polarization independent as compared to the other three types of meta-atoms. The designed DMAL can either be fully embedded in a low index substrate or partially uncovered. We study and discuss the partially uncovered case firstly and describe the fully embedded case at the following. Here, the uncovered part in DMAL is the PCML, which is designed with the GaN cylinders on an Al_2O_3 substrate. On the other hand, the PVML consists of the GaN cylinders embedded in the Al_2O_3 substrate. GaN and Al_2O_3 are chosen as the materials for our design because of their mature fabrication technologies in the LED industry [33]. The uniform meta-atom arrays are simulated using FDTD, and the transmissions and phase delays are obtained, as shown in Figs. 2(a)–(d). When the radius of the GaN cylinder varies from 25 nm to 75 nm, the phase delay covers 0-2π at one arbitrary wavelength in the range from 460 nm to 700 nm, and the transmission is high (> 0.9) in the same range. These properties are important for high-performance metalens design. Inset in Fig. 2(a) is the schematic of meta-atom with a 900 nm height (H = 900 nm) GaN cylinder on the Al_2O_3 substrate and inset in Fig. 2(c) is the 1,400 nm height (H = 1,400 nm) GaN cylinder embedded in the Al_2O_3 substrate. They are arranged in uniform arrays with a period (P) of 195 nm.

As the basic building blocks, the meta-atom directly affects the dispersion of a designed metalens. Therefore, the group delay ($\partial\varphi/\partial\lambda$) is analyzed based on the calculated phase delay of meta-atom uniform arrays in Fig. 2(e). It is discovered that the group delay is affected by the refractive index, the height of the cylinder and the period of the array as shown in Fig. 2(f) as well as Fig. 3. Although the dispersion of an arbitrary metalens could be obtained from the meta-atom properties through the superposing method [45], full-wave simulation method (FDTD) is employed to directly study the dispersion of metalens for convenience.

Optics EXPRESS

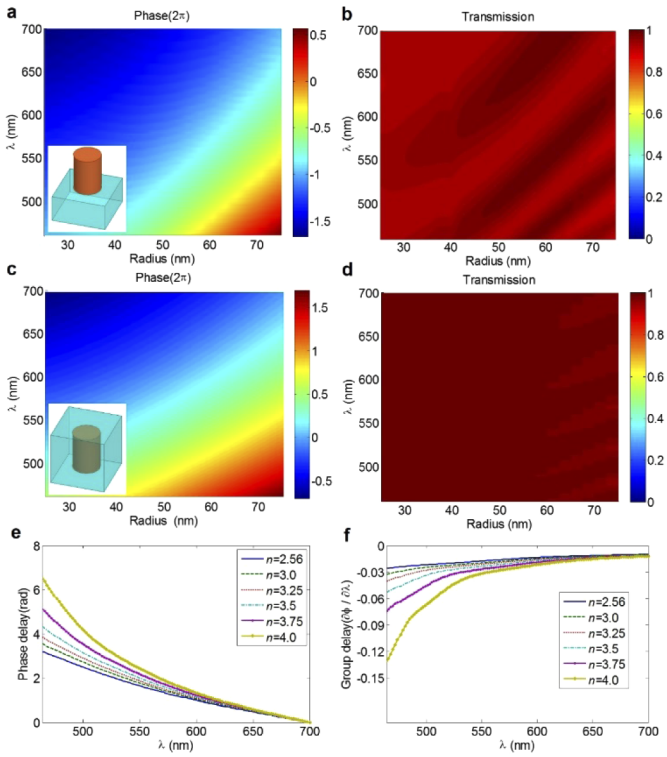

Fig. 2. Accumulated phase delay and transmission. (a) Accumulated phase delay and (b) transmission of the uniform meta-atom arrays ($P = 195$ nm) with GaN cylinders ($H = 900$ nm) on an Al_2O_3 substrate. Inset in (a) is the schematic of the uncovered meta-atom used for uncovered PCML design. (c) Accumulated phase delay and (d) transmission of the uniform meta-atom arrays ($P = 195$ nm) with GaN cylinders ($H = 1{,}400$ nm) embedded in an Al_2O_3 substrate. Inset in (c) is the schematic of the embedded meta-atom used for embedded PVML design. (e) Accumulated phase delay and (f) group delay of a series of uncovered meta-atom arrays ($H = 800$ nm, $R = 40$ nm, and $P = 195$ nm) with different refractive indices.

3.2. *Dispersion of single layer metalens*

To compensate for the dispersion of metalens, the single layer metalens' dispersion properties are first investigated. The meta-atoms are chosen as GaN ($n = 2.6$) cylinders on Al_2O_3 ($n = 1.55$) substrate. Following the phase profile in Eq. (1) and the phase delay of meta-atoms in Fig. 2(a), metalenses are designed and simulated for the dispersion investigation through focal length analysis. Two cases are simulated: (1) a PVML with focal length of $f_1 = 97.3$ μm and numerical aperture NA = 0.1, and (2) a PVML with $f_1 = 27.3$ μm and NA = 0.34. The normalized field amplitudes along the lens axis (z-axis) are plotted in Figs. 4(a) and (b), respectively. It can be seen that the focal length of the PVML is proportional to the wavelength ($\partial f/\partial\lambda > 0$) when the metalens has a simple hyperbolic phase profile only (refer to the inset curve in Fig. 4(a)), which means that the maximum phase difference on metalens is not larger than 2π. This type of dispersion is named as normal dispersion. When the metalens has a sawtooth liked phase profile (refer to the inset curve in Fig. 4(b)), the focal length of the PVML is inversely proportional to the wavelength ($\partial f/\partial\lambda < 0$) in the range from 460 nm to 700 nm, and a second focal spot appears in the range from 400 nm to 460 nm. This type of dispersion is named as abnormal dispersion. Similarly, the focal lengths of two PCMLs (with the same diameter and NA as the above PVMLs) are obtained via an adjoint simulation in which the fields are calculated by propagating an

Optics EXPRESS

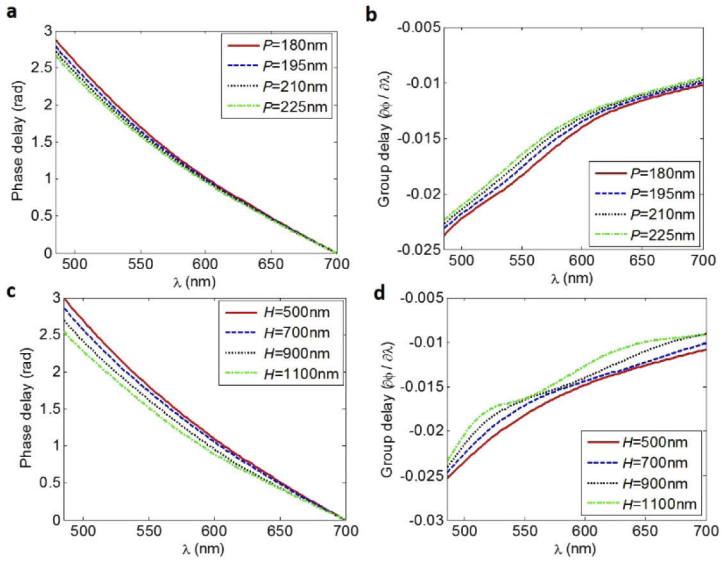

Fig. 3. Accumulated phase delay and group delay of meta-atoms. (a) Accumulated phase delay and (b) group delay of a series of uncovered GaN cylinder arrays ($H = 800$ nm, $R = 40$ nm, and $n = 2.56$) with different periods. (c) Accumulated phase delay and (d) group delay of a series of uncovered GaN cylinder arrays ($R = 40$ nm, $P = 195$ nm, and $n = 2.56$) with different heights.

electromagnetic wave in the opposite direction of the outgoing plane wave [43]. For single-layer PVML and PCML, their focal lengths in the wavelength range from 400 nm to 700 nm are shown in Figs. 4(c) and (d). It can be seen that reverse dispersion properties always exist between PVML and PCML for normal and abnormal dispersion cases.

The sawtooth liked phase profile of metalens leads to the second focal spot and abnormal dispersion. At the design wavelength, the discontinuity on the phase profile is exactly 2π, and it does not affect the lens functionality. For other wavelengths, the discontinuity is larger or smaller than 2π. Thus, the whole phase profile cannot recover to a perfect hyperbolic shape after several 2π phase shift. The whole metalens can be treated as several parts according to the phase profile discontinuity. The second focal spot and the abnormal dispersion are the interference results between these parts.

The PVML is separated into two parts, as shown in Fig. 5(a), (i).e., central and side parts as highlighted by red and green dashed lines. Then, we can equivalently replace the meta-atoms on the side with the perfect electrical conductor (PEC) to evaluate the performance of the meta-atoms in the central part (denoted as source S1). Similarly, we can replace the meta-atoms in the central part with PEC to evaluate the performance of the meta-atoms on the side parts (denoted as source S2).

As shown in Fig. 5(b), wave interference occurs at point P when two waves originate from source S_1 and source S_2 meet while traveling along with the same medium. r_1 and r_2 are the vectors from S_1 and S_2 to point P. The superposed wave equation at point P can be written as

$$y = y_1 + y_2 = A\cos(\omega t + \Delta\varphi), \tag{17}$$

$$\begin{cases} y_1 = A_1\cos(\omega t + \varphi_1 - k_0\hat{e}_1 \cdot \mathbf{r}_1) \\ y_2 = A_2\cos(\omega t + \varphi_2 - k_0\hat{e}_2 \cdot \mathbf{r}_2) \end{cases}, \tag{18}$$

Optics EXPRESS

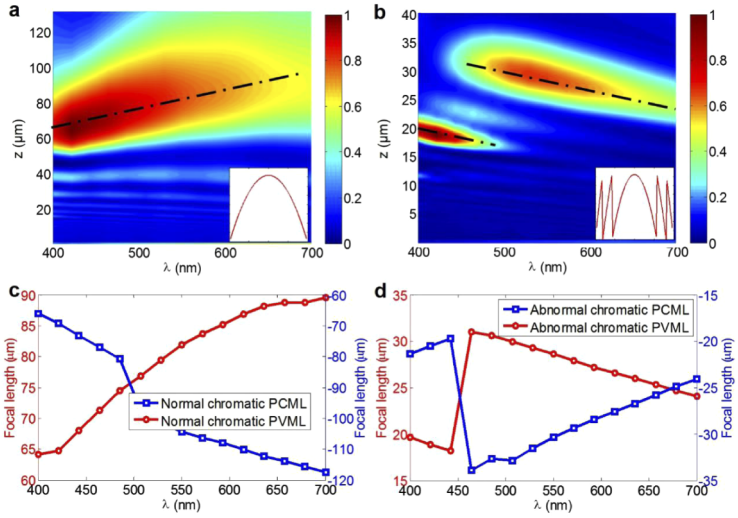

Fig. 4. Chromatic aberration of metalens. (a) The focal length of the PVML is increased from 65 to 90 μm within the bandwidth showing a normal dispersion. (b) The focal length of the PVML is decreased from 20 to 18μm and 32 to 24μm within the bandwidth showing an abnormal dispersion. A second focusing spot appears within 400 to 440 nm bandwidth for the PVML due to the inner couplings between the center and side parts. A reverse dispersion is shown for the (c) normal chromatic and (d) abnormal chromatic metalens.

where $A = \sqrt{{A_1}^2 + A_2^2 + 2A_1A_2\cos\Delta\varphi}$, $\Delta\varphi = \varphi_2 - \varphi_1 - \boldsymbol{k}_0 \cdot (\boldsymbol{r}_2 - \boldsymbol{r}_1)$, A_1 is the amplitude of field at point P produced by source S_1, A_2 is the amplitude of field at point P produced by source S_2, ω is the angular frequency, k_0 is wave number in free space, $\hat{e}_1$ is propagation direction unit vector of source S_1, $\hat{e}_2$ is propagation direction unit vector of source S_2. When the phase difference $\Delta\varphi$ is an even multiple of π, we will get a superposed field with a maximum amplitude of $A_{\max} = A_1 + A_2$, conversely a minimum amplitude of $A_{\min} = |A_1 - A_2|$ would be found when $\Delta\varphi$ is an odd multiple of π. Figures 5(c) and (d) show the field amplitude along the lens axis from the central (S_1) and side (S_2) parts of PVML. Figure 5(e) shows the cosine function of phase difference from two sources of S_1 and S_2, and minimum values can be found near the region of $z = 25$ to 35μm due to a destructive interference when the phase difference is an odd multiple of π. As a result, a jump of the focal length can be found near the region of $z = 25$ to 35μm in Figs. 5(f) and (g). The focal length is decreasing with the wavelengths, showing an abnormal dispersion. The simulation of Fig. 5(f) is from the analytical results of Eq. (1), which agrees well with the results from FDTD simulations in Fig. 5(g). This demonstrates that the second focal spot and abnormal dispersion is caused by destructive interference between the 0 - 2π phase profile of the central part and several 0 - 2π phase segments of the side parts.

In most cases, the focal length of the PVML and PCML is linear to the wavelength. Therefore, the dispersion ($\partial f/\partial\lambda$) can be represented by the effective Abbe number as derived in Eqs. (8) and (10). In the two equations, the effective Abbe number is a function of focal lengths at three pre-determined wavelengths, and directly linked to three effective refractive indices by Eq. (7). The effective refractive index of metalens is affected by the meta-atoms and their distributions [29]. For meta-atom with high refractive index cylinders, the design parameters include a refractive index, height, diameter and period. When the refractive index, height, and period of meta-atoms are fixed, the distribution is determined by the diameter D, the focal length f and the reference phase $\Delta\varphi$ of metalens. Here, the reference phase $\Delta\varphi$ is a unique parameter that does not affect the key performance (the focal length at the designed wavelength) of metalens, but

Optics EXPRESS

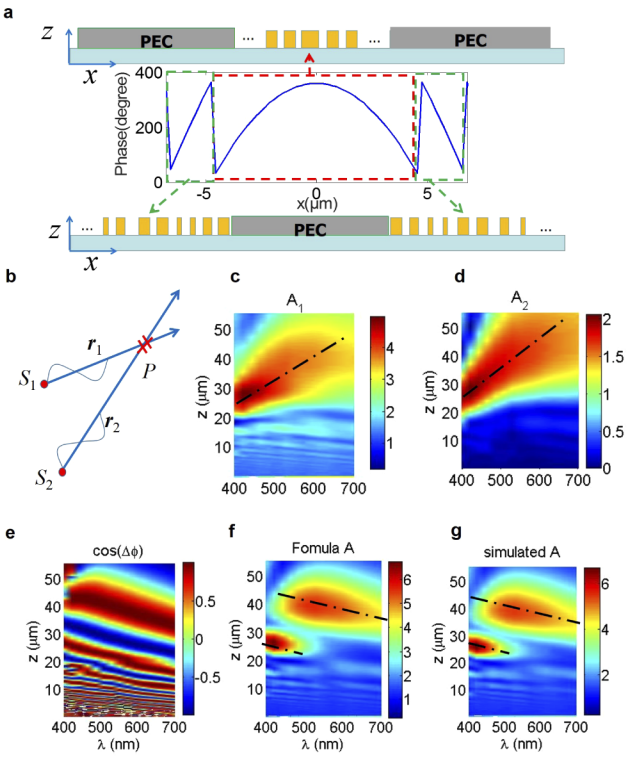

Fig. 5. Second focal spot and abnormal dispersion of PVML. (a) PVML is separated into two parts, i.e., central and side parts highlighted by dashed red and green dash lines. (b) Wave interference between S_1 and S_2. Field amplitude along lens axis from (c) S_1 and (d) S_2 of PVML. (e) Cosine function of phase difference from two sources of S_1 and S_2, minimum values can be found near the region of $z = 25$ to 35 due to a destructive interference when the phase difference is an odd multiple of π. Simulation of superposed field amplitude along the lens axis with (f) analytical formula Eq. (1) and (g) full-wave FDTD simulations.

affects the metalens' dispersion [26]. For abnormal dispersion, the effective Abbe number is a negative value based on Eqs. (8) or (10) ($f_F > f_C$). The larger absolute value of the effective Abbe number means smaller dispersion. If there is no dispersion ($f_F = f_C$), the effective Abbe number is infinite. The numerical simulation results show that, for the PVML with a focal length of 27.3 μm, its effective Abbe number varies from −1.78 to −3.15 when the reference phase change from 0° to 360° and the refractive index of the cylinder is 2.6. The varied range is increased to −1.77 to −9.44 when the refractive index is changed to 3.8 (see Fig. 6 for more details).

3.3. *Dual-layer achromatic metalens*

Here, we firstly demonstrate a partially uncovered DAML with a focal length of $f_t = 36$ μm and a diameter of $D = 19.5$ μm (NA ~ 0.26). To realize the DAML, the distance between two metalens (d) is fixed as 2 μm, and GaN ($n = 2.6$) cylinders embedded in Al_2O_3 ($n_3 = n_4 = 1.55$) are used as meta-atoms ($P = 195$ nm, $H = 1{,}400$ nm) for PVML design. In this design, the reference phase is fixed at zero ($\Delta\varphi = 0$) and the focal length is varied in a range from 8 μm to 30 μm (8 μm $\le f_1 \le$ 30 μm) with a step size of 1 μm. The corresponding effective Abbe number V_1 is obtained through full-wave simulation by using FDTD. Then, the corresponding optimal PCML design is determined by minimizing the dispersion of DMAL ($|\Delta'|$). Based on Eq. (11) and Eq. (16), the solution of f_2 and V_2 can be directly obtained. Although it is easy to design a

Optics EXPRESS

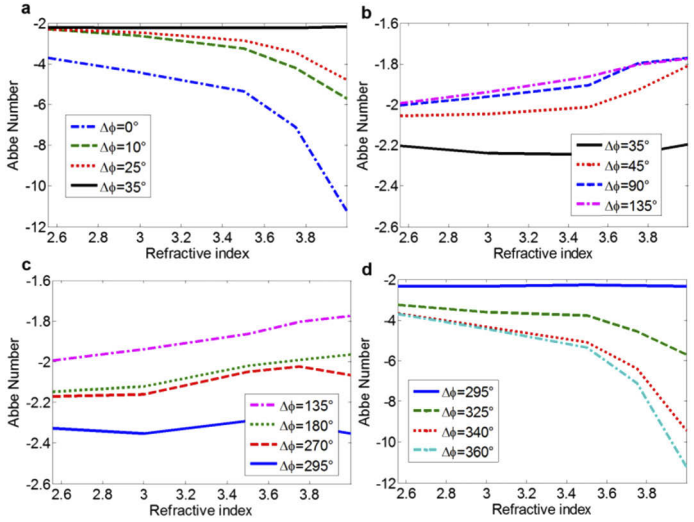

Fig. 6. Dispersion of PVML with respect to refractive index and reference phase. The effective Abbe number of PVML versus the reference phase $\Delta\varphi$ and the refractive index of the cylinders embedded in the Al_2O_3 substrate. The dispersion is increased when the reference phase changes from (a, b) 0° to 135°, but decreased from (c, d) 135° to 360°.

PCML with the focal length of f_2, it is difficult to ensure that it has the exact effective Abbe number V_2. Alternatively, a database is established, which includes all possible PCMLs with the designed meta-atoms (GaN cylinders on Al_2O_3 substrate, $P = 195$ nm, $450\text{ nm} \le H \le 1000$ nm, $25\text{ nm} \le r \le 75$ nm), zero reference phase ($\Delta\varphi = 0$), and the diameter of $D = 19.5$ μm. This database has a group of design pairs (f_2, V_2), and the pair with minimal dispersion is selected.

The final designed partially uncovered DAML consists of a PVML with a focal length of 15.6 μm and effective Abbe number of −4.33 ($f_1 = 15.6$ μm, $V_1 = -4.33$) and a PCML with a focal length of −27.3 μm and effective Abbe number of −3.24 ($f_2 = -27.3$ μm, $V_2 = -3.24$). The corresponding dispersion $|\Delta'|$ of DAML is 6.0×10^{-3} μm^{-1}. Compared to the single-layer chromatic metalens with the same focal length at design wavelength (592 nm), the designed DAML has much less dispersion as shown in Fig. 7. For instance, the single-layer chromatic metalens has a focal length difference of 36 μm when the wavelength changes from 460 nm to 700 nm. For the DAML, the focal length difference is just less than 2 μm. The simulated focusing efficiency of the DAML, which is defined as the ratio of the power of focal spot to the total incident power, is shown in Fig. 7(b). Maximum efficiency of 59% can be achieved at the designed center wavelength of 550 nm and average efficiency of 50% can be achieved across the bandwidth. The proposed DAML has a relatively lower efficiency with respect to the single-layer chromatic metalens, which is due to the additional losses induced by the PCML. It is possible to be improved by optimizing the design of each layer of metalens [45,46]. The simulated full width at half maximum (FWHM) of the focal spots of metalenses is shown in Fig. 7(c). Similar FWHM can be found for both the designed DAML and single layer chromatic metalens. The simulated field amplitude profiles of the focal spot at different wavelengths are shown in Figs. 7(d) and (e), respectively.

After that, a fully embedded DAML with a focal length of $f_t = 36$ μm and a diameter of $D = 19.5$ μm (NA ~ 0.26) is demonstrated. It consists of a PVML with a focal length of 15.6 μm and an effective Abbe number of −4.33 ($f_1 = 15.6$ μm, $V_1 = -4.33$) and a PCML with a focal length of −27.3 μm and effective Abbe number of −3.52 ($f_2 = -27.3$ μm, $V_2 = -3.52$). The corresponding dispersion $|\Delta'|$ of DAML is 6.8×10^{-3} μm^{-1}. Compared to the single-layer chromatic metalens

Optics EXPRESS

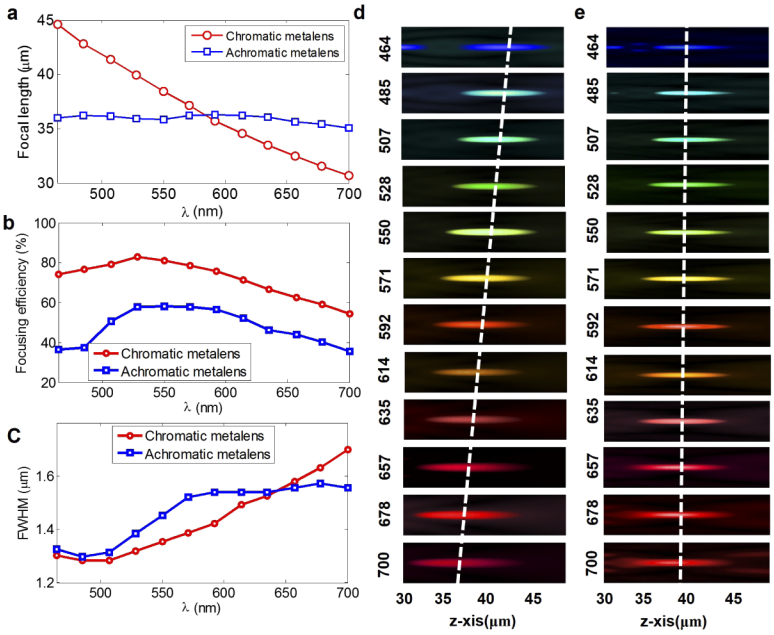

Fig. 7. Numerical results of single-layer chromatic metalens and designed DAML. (a) The focal length of chromatic metalens (red) and designed DAML (blue). (b) Focusing efficiency of chromatic metalens (red) and designed DAML (blue), which is defined as the power on focal spot normalized by the power of the incident beam. (c) The full width at half maximum (FWHM) of focal spots of the chromatic metalens (red) and the DAML (blue). Field amplitude distribution for (d) chromatic metalens and (e) designed DAML.

with the same focal length at the design wavelength (550 nm), the designed DAML has much less dispersion as shown in Fig. 8. For instance, the single-layer chromatic metalens has a focal length difference of 18 μm when the wavelength changes from 400 nm to 700 nm. For the DAML, the focal length difference is less than 1.5 μm. The simulated focusing efficiency of the DAML is shown in Fig. 8(b). The maximum efficiency of 55% can be achieved at the designed central wavelength of 550 nm and average efficiency of 42% can be achieved across the bandwidth. The simulated full width at half maximum (FWHM) of the focal spots of metalenses is shown in Fig. 8(c). Similar FWHM can be found for both the designed DAML and single layer chromatic metalens. The simulated field amplitude profiles of the focal spot for different wavelengths are shown in Fig. 8(d). The two designed DAML here are both cylindrical metalens. However, the proposed design method is also applicable for dual-layer circular achromatic metalens design.

It is possible to design a DAML with different NAs. Figures 9(a) and (b) shows the focal length of DAML with NA varies from 0.18 to 0.53 and Figs. 9(c) and (d) shows the corresponding focusing efficiencies. For NA smaller than 0.18, it is possible to design a DAML with good performance specifications. However, smaller NA means longer focal distance and larger simulation space. Therefore, cases with NA < 0.18 are not optimized and discussed in this paper due to limited computational capability. For NA larger than 0.53, the second focal spot appears, and the current dispersion compensation method does not include it for consideration yet. A modified method should be developed for higher NA cases. For a fixed PVML, slightly different PCMLs can be chosen to compensate for the dispersion. These results indicate that small fabrication imperfection has a slight impact on the focal length and the focusing efficiency. However, the DAML is still working. In previous cases, the distance d between the PCML and the PVML is fixed as 2 μm. The distance d only has slight effects on the achromatic performance

Optics EXPRESS

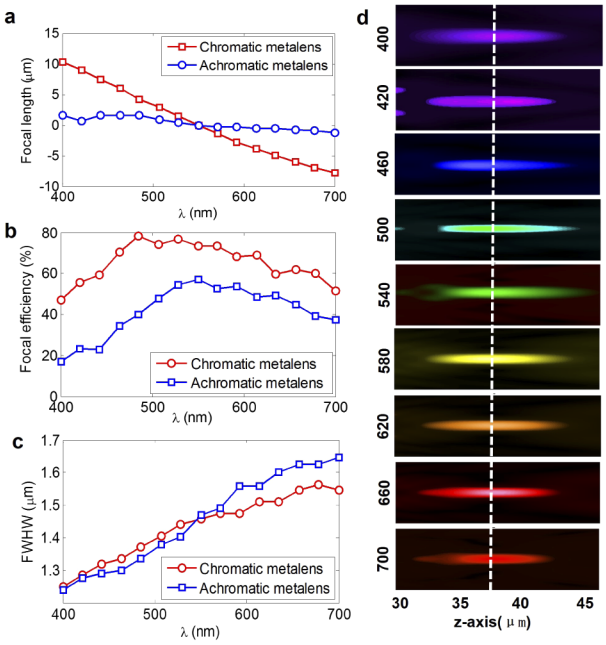

Fig. 8. Numerical results of single-layer chromatic metalens and DAML. (a) The focal length of the chromatic metalens (red) and designed DAML (blue). (b) Focusing efficiency of chromatic metalens (red) and designed DAML (blue), which is defined as the power on focal spot normalized by the power of the incident beam. (c) The full width at half maximum (FWHM) of focal spots of the chromatic metalens (red) and the DAML (blue). (d) Field amplitude distribution around focal spots for the designed DAML.

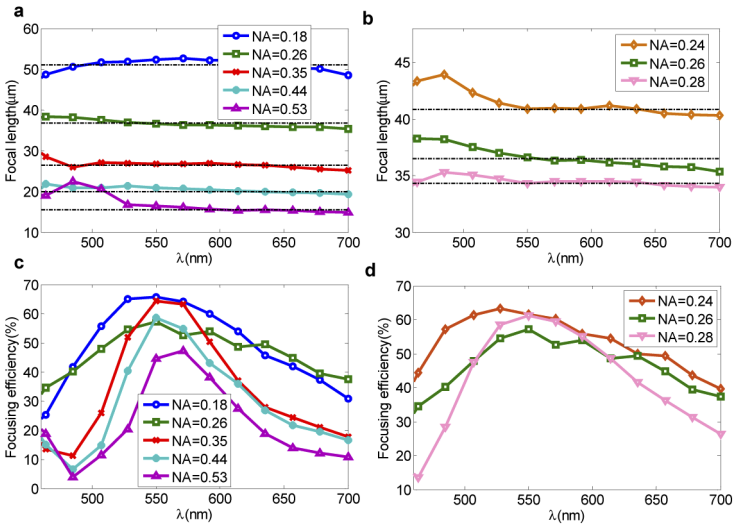

Fig. 9. The performance of designed DAML in the wavelength range from 460 nm to 700 nm. The focal length and the focusing efficiency of DAML versus wavelengths when NA varies in the range (a, c) from 0.18 to 0.53 and (b, d) from 0.24 to 0.28.

Optics EXPRESS

and focusing efficiency when $d > 1.8$ μm due to the weak near field coupling between the two layers, as shown in Fig. 10. Therefore, the designed DAML can be fabricated by using a mature multi-layer electron beam lithography method with a low index dielectric material as a spacer. It's also possible to be fabricated by using modified COMS fabrication technologies [47].

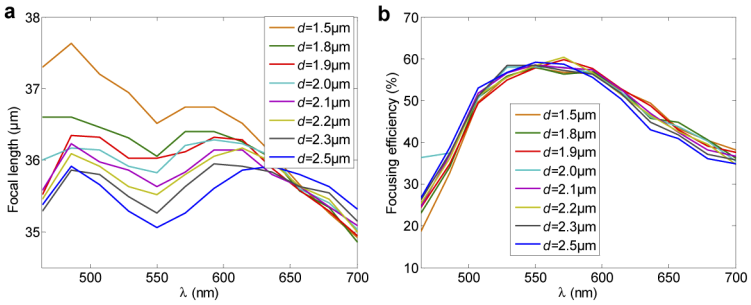

Fig. 10. Performance of designed DAML with different distances between PVML and PCML. (a) Focal length and (b) focal efficiency of the DAML with distance d range from 1,500 nm to 2,500 nm.

4. Conclusions

We have introduced an effective Abbe number for the dual-layer achromatic metalens design in this paper. The effective Abbe number represents the dispersions of PVML and PCML, which is affected by the meta-atoms and their distributions. The lens maker's equation is rewritten for the design and a pair of PVML and PCML with reverse dispersions is optimized to realize the DAML. By using this design method, a dual-layer achromatic metalens with simple cylindrical meta-atoms is demonstrated. The demonstrated DAML in visible wavelength has a similar focal length (difference < 2 μm), and an average focusing efficiency above 50%. Compared to the other design methods, our design method has no particular requirements on the meta-atoms. Therefore, we can choose simple and polarization-independent cylindrical meta-atoms for the achromatic metalens, paving the way for future multi-functional flat optics devices.

Funding

Fundamental Research Funds for the Central Universities (30918011103); Basic Research Program of Jiangsu Province (BK20171429); National Natural Science Foundation of China (61771246, 61871222, 61890540, 61890541).

Disclosures

The authors declare no conflicts of interest.

References

1. N. Yu and F. Capasso, "Flat optics with designer metasurfaces," Nat. Mater. **13**(2), 139–150 (2014).
2. H. T. Chen, A. J. Taylor, and N. Yu, "A review of metasurfaces: physics and applications," Rep. Prog. Phys. **79**(7), 076401 (2016).
3. S. B. Glybovski, S. A. Tretyakov, P. A. Belov, Y. S. Kivshar, and C. R. Simovski, "Metasurfaces: from microwaves to visible," Phys. Rep. **634**, 1–72 (2016).
4. S. Chang, X. Guo, and X. Ni, "Optical metasurfaces: progress and applications," Annu. Rev. Mater. Res. **48**(1), 279–302 (2018).
5. C. W. Qiu, W. X. Jiang, and T. J. Cui, "Electromagnetic metasurfaces: from concept to applications," Sci. Bull. **64**(12), 791–792 (2019).

Optics EXPRESS

6. K. Ou, G. Li, T. Li, H. Yang, F. Yu, J. Chen, Z. Zhao, G. Cao, X. Chen, and W. Lu, "High efficiency focusing vortex generation and detection with polarization-insensitive dielectric metasurfaces," Nanoscale **10**(40), 19154–19161 (2018).
7. G. Li, B. P. Clarke, J. K. So, K. F. MacDonald, and N. I. Zheludev, "Holographic free-electron light source," Nat. Commun. **7**(1), 13705 (2016).
8. X. Ni, S. Ishii, A. V. Kildishev, and V. M. Shalaev, "Ultra-thin, planar, Babinet-inverted plasmonic metalenses," Light: Sci. Appl. **2**(4), e72 (2013).
9. M. Khorasaninejad, W. T. Chen, R. C. Devlin, J. Oh, A. Y. Zhu, and F. Capasso, "Metalenses at visible wavelengths: Diffraction-limited focusing and subwavelength resolution imaging," Science **352**(6290), 1190–1194 (2016).
10. X. Ni, Z. J. Wong, M. Mrejen, Y. Wang, and X. Zhang, "An ultrathin invisibility skin cloak for visible light," Science **349**(6254), 1310–1314 (2015).
11. Y. F. Yu, A. Y. Zhu, R. Paniagua-Domínguez, Y. H. Fu, B. Luk'yanchuk, and A. I. Kuznetsov, "High–transmission dielectric metasurface with 2π phase control at visible wavelengths," Laser Photonics Rev. **9**(4), 412–418 (2015).
12. S. Liu, H. Chen, and T. J. Cui, "A broadband terahertz absorber using multi-layer stacked bars," Appl. Phys. Lett. **106**(15), 151601 (2015).
13. B. Yang, T. Liu, H. Guo, S. Xiao, and L. Zhou, "High-performance meta-devices based on multi-layer meta-atoms: interplay between number of layer and phase coverage," Sci. Bull. **64**(12), 823–835 (2019).
14. N. Yu, P. Genevet, M. A. Kats, F. Aieta, J. P. Tetienne, F. Capasso, and Z. Gaburro, "Light propagation with phase discontinuities: generalized laws of reflection and refraction," Science **334**(6054), 333–337 (2011).
15. X. Ni, N. K. Emani, A. V. Kildishev, A. Boltasseva, and V. M. Shalaev, "Broadband light bending with plasmonic nanoantennas," Science **335**(6067), 427 (2012).
16. H. Yang, G. Li, G. Cao, Z. Zhao, J. Chen, K. Ou, X. Chen, and W. Lu, "Broadband polarization resolving based on dielectric metalenses in the near-infrared," Opt. Express **26**(5), 5632–5643 (2018).
17. A. Arbabi, Y. Horie, M. Bagheri, and A. Faraon, "Dielectric metasurfaces for complete control of phase and polarization with subwavelength spatial resolution and high transmission," Nat. Nanotechnol. **10**(11), 937–943 (2015).
18. H. F. Ma, X. Chen, H. S. Xu, X. M. Yang, W. X. Jiang, and T. J. Cui, "Experiments on high-performance beam-scanning antennas made of gradient-index metamaterials," Appl. Phys. Lett. **95**(9), 094107 (2009).
19. D. Isakov, C. J. Stevens, F. Castles, and P. S. Grant, "3D–printed high dielectric contrast gradient index flat lens for a directive antenna with reduced dimensions," Adv. Mater. Technol. **1**(6), 1600072 (2016).
20. D. R. Smith, J. J. Mock, A. F. Starr, and D. Schurig, "Gradient index metamaterials," Phys. Rev. E **71**(3), 036609 (2005).
21. M. Khorasaninejad, F. Aieta, P. Kanhaiya, M. A. Kats, P. Genevet, D. Rousso, and F. Capasso, "Achromatic metasurface lens at telecommunication wavelengths," Nano Lett. **15**(8), 5358–5362 (2015).
22. E. Arbabi, A. Arbabi, S. M. Kamali, Y. Horie, and A. Faraon, "Multiwavelength polarization-insensitive lenses based on dielectric metasurfaces with meta-molecules," Optica **3**(6), 628–633 (2016).
23. O. Avayu, E. Almeida, Y. Prior, and T. Ellenbogen, "Composite functional metasurfaces for multispectral achromatic optics," Nat. Commun. **8**(1), 14992 (2017).
24. E. Arbabi, A. Arbabi, S. M. Kamali, Y. Horie, and A. Faraon, ""Multiwavelength metasurfaces through spatial multiplexing," Sci. Rep. **6**(1), 32803 (2016).
25. D. Lin, A. L. Holsteen, E. Maguid, G. Wetzstein, P. G. Kik, E. Hasman, and M. L. Brongersma, "Photonic multitasking interleaved Si nanoantenna phased array," Nano Lett. **16**(12), 7671–7676 (2016).
26. M. L. Tseng, H. H. Hsiao, C. H. Chu, M. K. Chen, G. Sun, A. Q. Liu, and D. P. Tsai, "Metalenses: advances and applications," Adv. Funct. Mater. **6**, 1800554 (2018).
27. V. C. Su, C. H. Chu, G. Sun, and D. P. Tsai, "Advances in optical metasurfaces: fabrication and applications," Opt. Express **26**(10), 13148–13182 (2018).
28. M. Khorasaninejad and F. Capasso, "Metalenses: Versatile multi-functional photonic components," Science **358**(6367), eaam8100 (2017).
29. M. Khorasaninejad, Z. Shi, A. Y. Zhu, W. T. Chen, V. Sanjeev, A. Zaidi, and F. Capasso, "Achromatic metalens over 60 nm bandwidth in the visible and metalens with reverse chromatic dispersion," Nano Lett. **17**(3), 1819–1824 (2017).
30. E. Arbabi, A. Arbabi, S. M. Kamali, Y. Horie, and A. Faraon, "Controlling the sign of chromatic dispersion in diffractive optics with dielectric metasurfaces," Optica **4**(6), 625–632 (2017).
31. S. Wang, P. C. Wu, V. C. Su, Y. C. Lai, C. H. Chu, J. W. Chen, S. H. Lu, J. Chen, B. Xu, C. H. Kuan, T. Li, S. Zhu, and D. P. Tsai, "Broadband achromatic optical metasurface devices," Nat. Commun. **8**(1), 187 (2017).
32. H.-H. Hsiao, Y. H. Chen, R. J. Lin, P. C. Wu, S. Wang, B. H. Chen, and D. P. Tsai, "Integrated resonant unit of metasurfaces for broadband efficiency and phase manipulation," Adv. Funct. Mater. **6**, 1800031 (2018).
33. S. Wang, P. C. Wu, V.-C. Su, Y.-C. Lai, M.-K. Chen, H. Y. Kuo, B. H. Chen, Y. H. Chen, T.-T. Huang, J.-H. Wang, R.-M. Lin, C.-H. Kuan, T. Li, Z. Wang, S. Zhu, and D. P. Tsai, "A broadband achromatic metalens in the visible," Nat. Nanotechnol. **13**(3), 227–232 (2018).
34. R. J. Lin, V. C. Su, S. Wang, M. K. Chen, T. L. Chung, Y. H. Chen, H. Y. Kuo, J. W. Chen, J. Chen, Y. T. Huang, and J. H. Wang, "Achromatic metalens array for full-colour light-field imaging," Nat. Nanotechnol. **14**(3), 227–231 (2019).

Optics EXPRESS

35. W. T. Chen, A. Y. Zhu, V. Sanjeev, M. Khorasaninejad, Z. Shi, E. Lee, and F. Capasso, "A broadband achromatic metalens for focusing and imaging in the visible," Nat. Nanotechnol. **13**(3), 220–226 (2018).
36. S. Shrestha, A. C. Overvig, M. Lu, A. Stein, and N. Yu, "Broadband achromatic dielectric metalenses," Light: Sci. Appl. **7**(1), 85 (2018).
37. E. Arbabi, A. Arbabi, S. M. Kamali, Y. Horie, and A. Faraon, "Miniature optical planar camera based on a wide-angle metasurface doublet corrected for monochromatic aberrations," Nat. Commun. **7**(1), 13682 (2016).
38. B. Groever, W. T. Chen, and F. Capasso, "Meta-lens doublet in the visible region," Nano Lett. **17**(8), 4902–4907 (2017).
39. W. T. Chen, A. Y. Zhu, J. Sisler, Y. W. Huang, K. M. Yousef, E. Lee, C. W. Qiu, and F. Capasso, "Broadband achromatic metasurface-refractive optics," Nano Lett. **18**(12), 7801–7808 (2018).
40. C. Kim, S. Kim, and B. Lee, "Doublet metalens design for high numerical aperture and simultaneous correction of chromatic and monochromatic aberrations," Opt. Express **28**(12), 18059–18076 (2020).
41. A. McClung, M. Mansouree, and A. Arbabi, "At-will chromatic dispersion by prescribing light trajectories with cascaded metasurfaces," Light: Sci. Appl. **9**(1), 93 (2020).
42. S. Molesky, Z. Lin, A. Y. Piggott, W. Jin, J. Vucković, and A. W. Rodriguez, "Inverse design in nanophotonics," Nat. Photonics **12**(11), 659–670 (2018).
43. T. Phan, D. Sell, E. W. Wang, S. Doshay, K. Edee, J. Yang, and J. A. Fan, "High-efficiency, large-area, topology-optimized metasurfaces," Light: Sci. Appl. **8**(1), 48 (2019).
44. L. Verslegers, P. B. Catrysse, Z. Yu, J. S. White, E. S. Barnard, M. L. Brongersma, and S. Fan, "Planar lenses based on nanoscale slit arrays in a metallic film," Nano Lett. **9**(1), 235–238 (2009).
45. D. Jia, Y. Tian, W. Ma, X. Gong, J. Yu, G. Zhao, and X. Yu, "Transmissive terahertz metalens with full phase control based on a dielectric metasurface," Opt. Lett. **42**(21), 4494–4497 (2017).
46. H. Chung and O. D. Miller, "High-NA achromatic metalenses by inverse design," Opt. Express **28**(5), 6945–6965 (2020).
47. T. Hu, Q. Zhong, N. Li, Y. Dong, Z. Xu, Y. H. Fu, D. Li, V. Bliznetsov, Y. Zhou, K. H. Lai, Q. Lin, S. Zhu, and N. Singh, "CMOS-compatible a-Si metalenses on a 12-inch glass wafer for fingerprint imaging," Nanophotonics **9**(4), 823–830 (2020).